3D Modelling of High Numerical Aperture Imaging in Thin Films

D. G. Flagello

IBM T.J. Watson Research Center
Yorktown Heights, N.Y. 10598

Tom Milster

Optical Science Center
Univerisity of Arizona
Tucson, Arizona 85721

Abstract

This paper describes a modelling technique used to explore three dimensional (3D) image irradiance distributions formed by high numerical aperture (NA > 0.5) lenses in homogeneous, linear films. This work uses a 3D modelling approach that is based on a plane-wave decomposition in the exit pupil. Each plane wave component is weighted by factors due to polarization, aberration, and input amplitude and phase terms. This is combined with a modified thin-film matrix technique to derive the total field amplitude at each point in a film by a coherent vector sum over all plane waves. Then the total irradiance is calculated. The model is used to show how asymmetries present in the polarized image change with the influence of a thin film through varying degrees of focus.

1. Introduction

The demand for highly integrated electronic devices has motivated investigation into better lens resolution in micro-photolithography. Lens resolution is roughly proportional to λ/NA; therefore, we desire to maximize NA and minimize λ. Photoresist, source, and lens materials issues limit the operating wavelength much below 248nm. NAs are design and budget limited, with a possible practical maximum of 0.95. In this paper, we will show that sophisticated models are needed to understand fundamentals of imaging in the high NA regime.

Traditional models used in micro-photolithography are based on scalar image formation under the Fresnel approximations[1]. The central approximation is to treat spherical lens and pupil surfaces as pure quadratic paraboloids. This holds in the low NA regime but it breaks down when the exit pupil diameter is of the same order as the distance from pupil to image, i.e., for NA $\geq$ 0.5. Furthermore, the traditional scalar models cannot treat polarization. They, in effect, assume that each plane-wave component has the same polarization amplitude, with polarization vectors parallel to one another and perpendicular to the axis. In a high NA system, there is significant variation of these vectors across the exit pupil. Each x, y, and z cartesian component has a different polarization contribution. Furthermore, these scalar models treat irradiance within the photoresist film as if the aerial image could be propagated through the film stack as a normally incident plane wave. This approximation is reasonable for NAs below 0.5 or 0.6, but at higher NAs, the propagation angles of the electric field (E) become significant.

One of the early experiments of Wiener[2] shows that, at oblique angles, light polarized parallel to the plane of incidence (P or TM polarization) exhibits reduced contrast in photographic film compared to light polarized perpendicular to the plane of incidence (S or TE polarization). For example, a pair of P-polarized plane waves propagating within a film at $\pm 45°$ produce no interference fringes because their E vectors are perpendicular to each other. Moreover, standing wave effects in the resist film stack are also different in the two polarizations. This is illustrated in Figure 1 with a plane wave incident

on a photoresist film over silicon at 33°, 44°, 58°, and 72° (or 0.55, 0.7, 0.85, and 0.95 NA respectively). The total power absorbed in the film, which is proportional to photoresist exposure, is ploted as a function of coated photoresist thickness in Figure 1. Although the differences between the polarizations are slight at 0.55 NA, they become appreciable high NAs. It becomes apparent that any imaging models for high NA must take into consideration the vector nature of light.

This work presents a 3D vector imaging model for homogeneous, linear, thin films. Previous work[3] concentrated on a 2D approach. Other authors[4-8] have looked at computationally intensive techniques for inhomogeneous films or required axially symmetric systems to obtain analytic solutions. In comparison, by limiting this work to homogeneous films, a technique can be presented that is easily visualized and computationally rapid. Since the final computation is numeric, no restriction is placed on the system symmetry. The model uses the Debye approach[9] to characterize the image field as a plane wave-decomposition. This restricts the propagation direction of the plane waves to the cone of rays subtended by the exit pupil of a high NA lens with its vertex at the geometrical focus. If a film stack is located at or near the focus, the amplitude and phase of each plane wave can be used as input into a thin-film matrix routine to calculate the local field in the top film. The total field is then the summation over all plane waves.

2. Model

Consider the Kohler projection system shown in Figure 2. It is assumed that the system is lossless, and has a Strehl ratio above 0.8. The film of interest is the 1st film, which is homogeneous and linear with thickness d_1. All optical elements from the source to the entrance pupil have low NA and can be modelled by traditional scalar methods. Additionally, the polarization remains constant throughout the optical system and is only altered at the exit pupil. These assumptions allow for a direct mapping of the amplitude and phase of the entrance pupil to the exit pupil of the imaging lens. In Figure 2, the source is initially polarized along the y axis. If a ray is considered to emerge from the exit pupil, it will now have polarization amplitudes for each cartesian component that depend on the exit pupil location.

The main assumption of this model is that each point in the exit pupil gives rise to a Huygens secondary spherical wavelet. If the image field size is much less than the pupil diameter and is located about the axis, the wavelets can be represented as plane waves propagating toward the the geometrical focus. Since each plane wave from an exit pupil point is normal to the localized surface about that point, the plane wave directions are limited to the cone (for circularly symmetric systems) formed by the vertex at the focus and the radius of the pupil. This is the Debye diffraction approach[9]. In the cases considered here, a local field size less than 10μm about the axis is sufficient to encompass all object points contributing significant amplitude to features of interest.

In Figure 3 we illustrate a general propagation vector, $\vec{k}$, for a plane-wave as

$$\begin{aligned}\vec{k} &= k_0\eta(\cos\phi\sin\theta\,\hat{x} + \sin\phi\sin\theta\,\hat{y} + \cos\theta\,\hat{z}) \\ &= k_0\eta(\alpha\,\hat{x} + \beta\,\hat{y} + \gamma\,\hat{z}) \quad ,\end{aligned} \qquad [1]$$

where k_0 is the free space propagation constant , and η is the defined as complex index of refraction given by

$$\eta = n - i\kappa \quad ,$$

where n is the real part of the refractive index and κ is the extinction coefficient.

Since θ is defined as the angle that $\vec{k}$ makes with the z axis and ϕ as the angle that the projection of $\vec{k}$ on the x-y plane makes with the x axis, the direction cosines have the standard definitions:

$$\alpha = \cos\phi\sin\theta$$

$$\beta = \sin\phi\sin\theta$$

$$\gamma = \cos\theta$$

$$\gamma = \sqrt{1 - \alpha^2 - \beta^2} \quad .$$

Propagation of a plane wave to the 1st film is illustrated by Figure 4. The pupil is given as a surface in direction cosine space over the variables (α, β). Since $z = 0$ at the center of curvature of the exit pupil, the direction of each plane-wave eminating from the exit pupil location (α_0, β_0) is completely defined by (α_0, β_0). A coordinate z' is defined as

$$z' = z - z_0 \quad . \qquad [2]$$

where z_0 is the distance from the geometrical focus of the system to the top surface of the film stack referenced to the incident medium. This places the top film surface at $z' = 0$ and the geometrical focus in the incident medium at $z' = -z_0$ or $z = 0$. If no aberrations are present in the optical system, all plane waves from the pupil are in phase at $z = 0$. Each plane wave will have a phase of $-k_0\eta_0\gamma_0 z_0$ at $z = z_0$, where subscripts on α_0, β_0, γ_0, and η_0 reference the incident medium. Also, the position vector, $\vec{r}$, has its origin at the top film surface, and the propagation vector in air, k_0, is coplanar with the refracted propagation vector in the film, k_1.

Each monochromatic plane wave propagating from the pupil to the top surface of the film has the form (with the periodic time factor $e^{i\omega t}$ suppressed)

$$\vec{E}(\alpha, \beta) = \vec{E}_{if}(\alpha, \beta)\, e^{-i\vec{k}_0 \cdot \vec{r}} = E_0(\alpha, \beta)\sqrt{\gamma_0}\; e^{ik_0 W(\alpha, \beta)}\; e^{-ik_0\eta_0\gamma_0 z_0}\; \vec{P}(\alpha, \beta)\; e^{-i\vec{k}_0 \cdot \vec{r}} \quad , \qquad [3]$$

and

$$\vec{k}_0 \cdot \vec{r} = k_0 \eta_0 (\alpha_0 x + \beta_0 y + \gamma_0 z') \quad .$$

$E_0(\alpha, \beta)$ describes the amplitude and phase on the entrance pupil due to the object diffraction. It is a scalar term due to the initial assumption of low NA on the object side. The $\sqrt{\gamma}$ term is arises from the requirement that the system has negligible energy losses and is aplanatic. It is derived[6] using the conservation of energy law, and it results in a complex amplitude at the exit pupil of $E_0(\alpha, \beta)\sqrt{\gamma_0}$. The next exponential term describes any residual aberration in terms of a wavefront phase error, $W(\alpha, \beta)$. Following this is the phase term due to the location of the top surface of the film. $\vec{P}(\alpha, \beta)$ is the polarization vector amplitude distribution across the exit pupil. It can be derived in terms of the propagation vector[10], k_0, since at all times it is assumed that the polarization vector is perpendicular to the propagation vector. Prior to the imaging lens, the initial polarization vector of the electric field is in some state of polarization that can be treated in terms of a orthogonal decomposition in x and y. Therefore, one only needs to examine the incoming component polarization vectors along the x or y axis. After passing through the lens, a given ray will have its polarization vector rotated accordingly. The cartesian components are found by applying the appropriate coordinate transformations. Upon interaction with the thin film surface, a plane of incidence about the z axis can be defined by the angle ϕ. This allows the components of the polarization vector to be further reduced in terms of contributions due to a component perpendicular to the plane of incidence, S or TE, and parallel to this plane, P or TM. Table I shows the values of the polarization amplitudes for each component. Note that $P_x^2 + P_y^2 + P_z^2 = 1$ and that the z component is only comprised of P polarization.

Figure 5 illustrates a plane wave from the pupil with amplitude and phase $\vec{E}_{if}(\alpha, \beta)$, described by Equation 3, arriving at the top surface of the film, interface I. The total field at any x,y,z point within the top film is found by summing the downward and upward fields at that location. The derivation presented here departs from the typical thin film-methods by presenting this in terms of the fields at bottom of the film, interface II, and then relating the result to the incident field at interface I through matrix formalism. The incident and reflected fields at interface II give for the field in the 1st film,

$$\text{Downward Field,} \quad \vec{E}^{+}(\alpha, \beta) = \vec{E}_{if}(\alpha, \beta)\; e^{ik_0 \eta_1 (\alpha_1 x + \beta_1 y + \gamma_1 z'')} \quad , \qquad [4]$$

$$\text{Upward Field,} \quad \vec{E}^{-}(\alpha, \beta) = \vec{E}_{rf}(\alpha, \beta)\; e^{ik_0 \eta_1 (\alpha_1 x + \beta_1 y - \gamma_1 z'')} \quad , \qquad [5]$$

where $z'' = d_1 - z'$.

The following relationships are found from Snell's law in direction cosine notation:

$$\begin{aligned} \eta_1 \alpha_1 &= \eta_0 \alpha_0 \\ \eta_1 \beta_1 &= \eta_0 \beta_0 \end{aligned} \quad , \tag{6}$$

and

$$\eta_1 \gamma_1 = \sqrt{\eta_1^2 - \eta_0^2 \sin^2(\cos^{-1}\gamma_0)} \quad . \tag{7}$$

The total field is given as

$$\begin{aligned} \vec{E}_T(\alpha, \beta) &= \vec{E}^+(\alpha, \beta) + \vec{E}^-(\alpha, \beta) \\ &= e^{ik_0 \eta_0 (\alpha_0 x + \beta_0 y)} \left(\vec{E}_{if}(\alpha, \beta)\, e^{i\Phi(z'')} + \vec{E}_{rf}(\alpha, \beta)\, e^{-i\Phi(z'')} \right) , \end{aligned} \tag{8}$$

where

$$\Phi(z'') = k_0 z'' \sqrt{\eta_1^2 - \eta_0^2 \sin^2(\cos^{-1}\gamma_0)} \quad . \tag{9}$$

The amplitudes in Equation 8 are related to the incident field by using thin-film matrix techniques to derive reflection and transmission coefficients for the full film stack and a partial film stack. Since the basics of this technique[11,12] are well known, only the novel mathematics pertaining to the current discussion will be presented. It is assumed that the index of refraction above the first surface, η_0, is real, and that the film in question is the first film layer on an arbitrary film stack. Using the notation in Hecht[13], a matrix can be defined for each film, j, by

$$M_j = \begin{bmatrix} \cos\delta_j & \dfrac{i \sin\delta_j}{Y_j} \\ iY_j \sin\delta_j & \cos\delta_j \end{bmatrix} , \tag{10}$$

where Y_j is defined as the effective index for S and P polarization and δ_j is the phase for a film thickness d_j, given by

$$\begin{aligned} Y_{jS} &= \eta_j \gamma_j \\ Y_{jP} &= \frac{\eta_j}{\gamma_j} \\ \delta_j &= k_0 \eta_j d_j \gamma_j \quad . \end{aligned} \tag{11}$$

A total M matrix can be defined that is the product of all the individual film matrices, as well as a partial M′ matrix that represents the film stack without the contribution of the 1st film:

$$\text{Total Matrix,} \qquad M = \prod_{j=1}^{j=s} M_j = \begin{bmatrix} m_{11} & m_{12} \\ m_{21} & m_{22} \end{bmatrix} , \tag{12}$$

and

$$\text{Partial Matrix,} \qquad M' = \prod_{j=2}^{j=s} M_j = \begin{bmatrix} m'_{11} & m'_{12} \\ m'_{21} & m'_{22} \end{bmatrix} . \qquad [13]$$

With respect to Figure 5, the reflection and transmission vector coefficients for the full film stack, $\vec{r}$ and $\vec{\tau}$ respectively, and at the 2nd interface, $\vec{r}_{II}$ and $\vec{\tau}_{II}$, can be defined with components given by

$$\tau = \tau_x = \tau_y = \frac{E_{\tau sx}}{E_{ilx}} = \frac{E_{\tau sy}}{E_{ily}} \qquad \tau_z = \frac{E_{\tau sz}}{E_{ilz}} , \qquad [14]$$

$$\tau_{II} = \tau_{IIx} = \tau_{IIy} = \frac{E_{\tau sx}}{E_{iIIx}} = \frac{E_{\tau sy}}{E_{iIIy}} \qquad \tau_{IIz} = \frac{E_{\tau sz}}{E_{iIIz}} , \qquad [15]$$

$$r = r_x = r_y = \frac{E_{rlx}}{E_{ilx}} = \frac{E_{rly}}{E_{ily}} \qquad r_z = \frac{E_{rlz}}{E_{ilz}} , \qquad [16]$$

and

$$r_{II} = r_{IIx} = r_{IIy} = \frac{E_{rIIx}}{E_{iIIx}} = \frac{E_{rIIy}}{E_{iIIy}} \qquad r_{IIz} = \frac{E_{rIIz}}{E_{iIIz}} , \qquad [17]$$

where the original assumption of film homogeneity and linearity has been invoked to allow the equality of the x and y coefficients.

The coefficients can be expanded following a similar treatment outlined in Hecht in terms of the M and M' matrix elements,

$$\tau = \frac{2Y_0}{Y_0 m_{11} + Y_0 Y_s m_{12} + m_{21} + Y_s m_{22}} \qquad \tau_{II} = \frac{2Y_1}{Y_1 m'_{11} + Y_1 Y_s m'_{12} + m'_{21} + Y_s m'_{22}} \qquad [18]$$

$$r = \frac{Y_0 m_{11} + Y_0 Y_s m_{12} - m_{21} - Y_s m_{22}}{Y_0 m_{11} + Y_0 Y_s m_{12} + m_{21} + Y_s m_{22}} \qquad r_{II} = \frac{Y_1 m'_{11} + Y_1 Y_s m'_{12} - m'_{21} - Y_s m'_{22}}{Y_1 m'_{11} + Y_1 Y_s m'_{12} + m'_{21} + Y_s m'_{22}} , \qquad [19]$$

where the dependence of the coefficients on α and β is given by Equation 11.

Propagating plane waves in the top film, which are represented by Equations 4 and 5, must also be solutions to the homogeneous wave equation and, therefore, Maxwell's equations. In particular, for a charge free media, it is required that the divergence of the field is zero in the incident medium and the film in question, hence

$$\vec{\nabla} \cdot \vec{E} = \vec{k} \cdot \vec{E} = 0 . \qquad [20]$$

Equations 6 and 14 for the incident medium give

$$\vec{k}_0 \cdot \vec{E}_{il} = \eta_0 (\alpha_0 E_{ilx} + \beta_0 E_{ily} + \gamma_0 E_{ilz}) = \frac{\eta_0 (\alpha_0 E_{\tau sx} + \beta_0 E_{\tau sy})}{\tau} + \frac{\eta_0 \gamma_0 E_{\tau sz}}{\tau_z} = 0 , \qquad [21]$$

which gives

$$\eta_0 (\alpha_0 E_{\tau sx} + \beta_0 E_{\tau sy}) = -\frac{\tau \eta_0 \gamma_0 E_{\tau sz}}{\tau_z} \quad . \tag{22}$$

Equation 20 for the downward field in the film and equation 22 give

$$\begin{aligned} \vec{k}_1 \cdot \vec{E}^+ &= \eta_1 (\alpha_1 E_{ifx} + \beta_1 E_{ify} + \gamma_1 E_{ifz}) \\ &= \frac{\eta_0 (\alpha_0 E_{\tau sx} + \beta_0 E_{\tau sy})}{\tau_{//}} - \frac{\eta_1 \gamma_1 E_{\tau sz}}{\tau_{//z}} \\ &= \frac{-\tau \eta_0 \gamma_0 E_{\tau sz}}{\tau_z \tau_{//}} - \frac{\eta_1 \gamma_1 E_{\tau sz}}{\tau_{//z}} = 0 \quad . \end{aligned} \tag{23}$$

Therefore,

$$\frac{\tau_z}{\tau_{//z}} = \frac{\tau}{\tau_{//}} \frac{\eta_0 \gamma_0}{\eta_1 \gamma_1} \quad . \tag{24}$$

Similarly, for the upward field,

$$\vec{k}_1 \cdot \vec{E}^- = \eta_1 (\alpha_1 E_{rfx} + \beta_1 E_{rfy} - \gamma_1 E_{rfz}) = r_{//} \eta_1 (\alpha_1 E_{ifx} + \beta_1 E_{ify}) - r_{//z} \eta_1 \gamma_1 E_{ifz} = 0 \quad . \tag{25}$$

By Equation 23,

$$\eta_1 (\alpha_1 E_{ifx} + \beta_1 E_{ify}) = -\eta_1 \gamma_1 E_{ifz} \quad . \tag{26}$$

Then, by substituting Equation 26 into 25,

$$r_{//} \eta_1 \gamma_1 E_{ifz} = -r_{//z} \eta_1 \gamma_1 E_{ifz} \quad , \tag{27}$$

and,

$$r_{//z} = -r_{//} \quad . \tag{28}$$

Finally, using Equations 3, 14-17, 24, and 28, Equation 8 can be given for each cartesian component, linking the thin film field with each plane wave emanating from the pupil, that is,

$$E_{Tx}(\alpha, \beta) = e^{ik_0 \eta (\alpha x + \beta y)} e^{-ik_0 \eta \gamma z_0} E_0(\alpha, \beta) \sqrt{\gamma} e^{ik_0 W(\alpha, \beta)} P_x(\alpha, \beta) \frac{\tau}{\tau_{//}} (e^{i\Phi(z')} + r_{//} e^{-i\Phi(z')}) \quad , \tag{29}$$

$$E_{Ty}(\alpha, \beta) = e^{ik_0 \eta (\alpha x + \beta y)} e^{-ik_0 \eta \gamma z_0} E_0(\alpha, \beta) \sqrt{\gamma} e^{ik_0 W(\alpha, \beta)} P_y(\alpha, \beta) \frac{\tau}{\tau_{//}} (e^{i\Phi(z')} + r_{//} e^{-i\Phi(z')}) \quad , \tag{30}$$

and

$$E_{Tz}(\alpha, \beta) = e^{ik_0 \eta (\alpha x + \beta y)} e^{-ik_0 \eta \gamma z_0} E_0(\alpha, \beta) \sqrt{\gamma} e^{ik_0 W(\alpha, \beta)} P_z(\alpha, \beta) \frac{\tau}{\tau_{//}} \frac{\eta \gamma}{\eta_1 \gamma_1} (e^{i\Phi(z')} - r_{//} e^{-i\Phi(z')}) \quad , \tag{31}$$

where α, β, γ, and η are referenced to the incident medium.

Since reflection and transmission coefficients are only defined in terms of either the S or P orientation, Equations 29-31 are further reduced into S and P components. The total field at any point within the 1st film is then given by the component sum of $\vec{E}_T(\alpha, \beta)$ due to the S contributions and the P contributions over the solid angle subtended by the pupil. The normalized field is given by

$$\vec{E}(x,y,z) = K\int_{\Omega}\vec{E}_{TS}(\alpha,\beta)\,d\Omega + K\int_{\Omega}\vec{E}_{TP}(\alpha,\beta)\,d\Omega \quad , \tag{32}$$

where K is a the normalization constant.

Since the differential solid angle can be written as

$$d\Omega = \frac{d\alpha\,d\beta}{\gamma} \quad , \tag{33}$$

the final expanded form for the local electric field components in a film is:

$$\begin{aligned} E_x(x,y,z) = K\int_{\alpha}\int_{\beta} & \frac{E_0(\alpha,\beta)\,P_{xS}(\alpha,\beta)\,e^{ik_0W(\alpha,\beta)}}{\sqrt{\gamma}}\,e^{ik_0\eta(\alpha x+\beta y-\gamma z_0)}\,\frac{\tau_S}{\tau_{IIS}}\,(e^{i\Phi(z'')} + r_{IIS}\,e^{-i\Phi(z'')})\,d\alpha\,d\beta \\ + K\int_{\alpha}\int_{\beta} & \frac{E_0(\alpha,\beta)\,P_{xP}(\alpha,\beta)\,e^{ik_0W(\alpha,\beta)}}{\sqrt{\gamma}}\,e^{ik_0\eta(\alpha x+\beta y-\gamma z_0)}\,\frac{\tau_P}{\tau_{IIP}}\,(e^{i\Phi(z'')} + r_{IIP}\,e^{-i\Phi(z'')})\,d\alpha\,d\beta \end{aligned} \tag{34}$$

$$\begin{aligned} E_y(x,y,z) = K\int_{\alpha}\int_{\beta} & \frac{E_0(\alpha,\beta)\,P_{yS}(\alpha,\beta)\,e^{ik_0W(\alpha,\beta)}}{\sqrt{\gamma}}\,e^{ik_0\eta(\alpha x+\beta y-\gamma z_0)}\,\frac{\tau_S}{\tau_{IIS}}\,(e^{i\Phi(z'')} + r_{IIS}\,e^{-i\Phi(z'')})\,d\alpha\,d\beta \\ + K\int_{\alpha}\int_{\beta} & \frac{E_0(\alpha,\beta)\,P_{yP}(\alpha,\beta)\,e^{ik_0W(\alpha,\beta)}}{\sqrt{\gamma}}\,e^{ik_0\eta(\alpha x+\beta y-\gamma z_0)}\,\frac{\tau_P}{\tau_{IIP}}\,(e^{i\Phi(z'')} + r_{IIP}\,e^{-i\Phi(z'')})\,d\alpha\,d\beta \end{aligned} \tag{35}$$

$$E_z(x,y,z) = K\int_{\alpha}\int_{\beta}\frac{E_0(\alpha,\beta)\,P_{zP}(\alpha,\beta)\,e^{ik_0W(\alpha,\beta)}}{\sqrt{\gamma}}\,e^{ik_0\eta(\alpha x+\beta y-\gamma z)}\,\frac{\tau_P\eta\gamma}{\tau_{IIP}\eta_1\gamma_1}\,(r_{IIP}\,e^{-i\Phi(z'')} - e^{i\Phi(z'')})\,d\alpha\,d\beta\,. \tag{36}$$

The limits of integration for circularly symmetric systems extend from -NA to NA with the requirement that

$$\sqrt{\alpha^2+\beta^2} \le NA \quad . \tag{37}$$

The localized irradiance at any point within the film can be expressed as,

$$I(x,y,z) = [\vec{E}(x,y,z)\cdot\vec{E}^{*}(x,y,z)]\,Re(\eta_1) = (\,|E_x(x,y,z)|^2 + |E_y(x,y,z)|^2 + |E_z(x,y,z)|^2\,)\,Re(\eta_1)\,. \tag{38}$$

This equation is easily evaluated numerically. The minimum sampling size can be determined either by trial and error, looking for convergence of the image, or by recognizing that Equations 34-36 represent a Fourier transform. If the image function is band limited within the image field, then by sampling theory[14], the image field sizes, X and Y, are inversely proportional to the sampling in the pupil. The minimum direction cosine interval can then be written as

$$\Delta\alpha = \frac{\lambda}{X}$$
$$\Delta\beta = \frac{\lambda}{Y} \quad [39]$$

In the cases of interest in this work the field size is limited to $5\mu m$ at $\lambda = 248nm$ giving $\Delta\alpha = 0.05$ For a 0.95 NA circularly symmetric system this results in 1100 samples in the pupil, i.e., only 1100 plane waves are needed to create the image within a film. This number is much less than other imaging models based on plane-to-plane propagation.

3. Results

Equation 38 was evaluated using a wavelength of $\lambda = 248nm$ and an incident medium of air with the wavefront aberration set to $W(\alpha, \beta) = 0$. Initially, the image of a point, or the point spread function (PSF), was computed for a non-absorbing photoresist film of $\eta_1 = 1.8$ on a matched substrate for an NA of 0.95. Figure 6 shows the normalized iso-irradiance contours for meridional slices along x and y for an initial source polarized along y and $z_0 = -.2\mu m$. Due to a significant z component contribution, the y slice is slightly wider than x and the interference effects are also less pronounced. This results in an asymmetry of the PSF in the x-y plane. There is also some asymmetry about the image in depth. This is explained by the spherical aberration caused by the top film surface. By Snell's law, the marginal ray at 0.95 NA will cross the optical axis at the bottom of the film or $z' = 1\mu m$. However, any paraxial ray will cross the axis at approximately $z' = .45\mu m$. The difference between these represents the longitudinal spherical aberration. The fact that most of the power is centered around a depth of $0.5\mu m$ is probably due to the smaller amplitude of the marginal plane waves from reflection losses at high angles and the greater number of paraxial plane waves .

Figure 7 shows a comparison of a the film PSF using a 0.6 and 0.95 NA system. The film is moderately absorbing with $\eta_1 = 1.8 - .04i$ over a silicon substrate with $\eta_s = 1.7 - 3.38i$. For each NA, the film surface is offset to result in the marginal ray crossing the axis at a depth of $0\mu m$ (no offset), $0.5\mu m$, and $1\mu m$. Since the substrate is no longer matched, standing wave interference patterns are observed. Decay of the irradiance due to absorption is also observed. The effects of polarization are more apparent at 0.95 NA, as evidenced by the difference in behavior between the x and y slices.

A tri-bar object with 0.17 lines and 0.17 spaces parallel to the x axis is shown in Figure 8a. The film, substrate, and z_0 offsets are identical to the previous 0.95 NA example. The resultant y meridional slice images using a 0.95 NA system are presented in Figures 8b-8d for x and y polarizations. Again, interference effects are less with the y polarization due to the influence of the z component. In Figure 8b the onset of spurious resolution is seen at the bottom of the film by the presence of four major irradiance lobes instead of three. The bending nature of the iso-irradiance contours are clearly the result of the vectorial nature of this model. Figure 9 shows a plot of the irradiance about the zero position at a depth of $z' = 0$ for the images in Figure 8b. Differences such as these become relevant in micro-lithography since the tolerances on the total processed structures maintained in photoresist must not exceed ± 10%.

4. Conclusion

A vector imaging model for thin films has been presented that is based on a plane wave decomposition of the radiation that propagates from the pupil, and a thin-film treatment of propagation into the film stack. The model is valid for NAs approaching unity and and tends to minimize the number of plane waves needed for an image. It is shown that, when the illumination is polarized, asymmetries are created due to high-NA polarization effects and spherical aberration caused by a film surface. The image iso-irradiance contours that are presented illustrate the vectorial nature of the model.

5. References

1 J. W. Goodman, Introduction to Fourier Optics (McGraw-Hill, 1968).

2 O. Wiener, Ann. d. Physik, 40 (1890), 203.

3 D. Flagello, A.E. Rosenbluth, C. Progler, and J. Armitage, Microcircuit Engineering 1991 (Elsevier Science)

4 M. Mansuripur, J. Opt. Soc. Am. A 6, 786-805 (1989).

5 M. Mansuripur, J. Appl. Phys. 67, 6466-6475 (1990).
6 B. Richards and E. Wolf, Proc. Royal Soc. A, 358 (1959).
7 M. Yeung, SPIE J., 922, 149-167 (1988).
8 J. J. Stamnes, Waves in Focal Regions (Adam Hilger, 1986).
9 M. Born and E. Wolf, Principles of Optics (Pergamon Press, 1980).
10 M. Mansuripur, J. Opt. Soc. Am A 3, 2086-2093 (1986).
11 P.H. Berning, Physics of Thin Films, G. Hass, Ed. (Academic Press 1963), 69-121.
12 H. A. MaCleod, Thin-Film Optical Filters (McGraw-Hill, 1989).
13 E. Hecht and A. Zajac Optics (Addeson-Wesley, 1979).
14 J. Gaskill, Linear Systems, Fourier Transforms, and Optics (John Wiley and Sons, 1978).

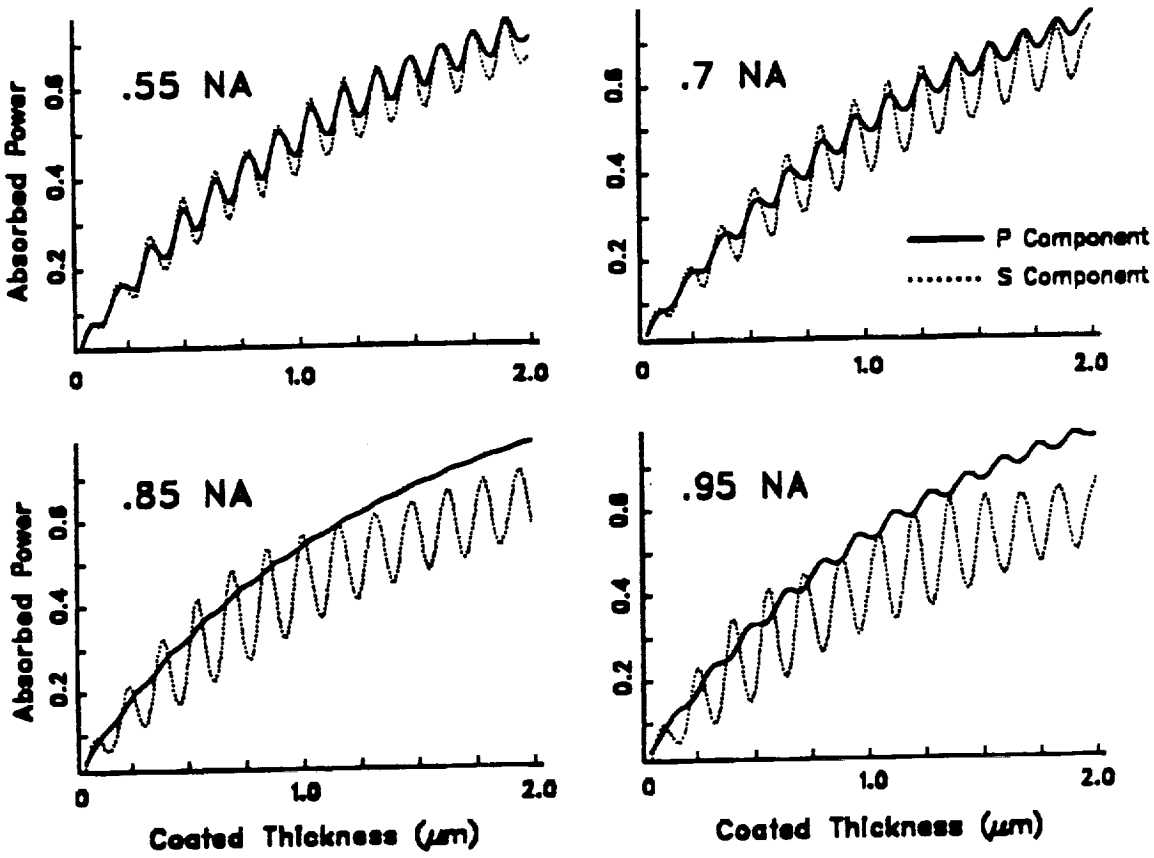

Fig. 1. Total absorbed power of an incident plane wave as a function of coated photoresist thickness for a moderately absorbing photoresist over a silicon substrate at $\lambda = 436nm$ The angle of incidence, θ, is given as the NA in air, i.e. $\sin\theta$

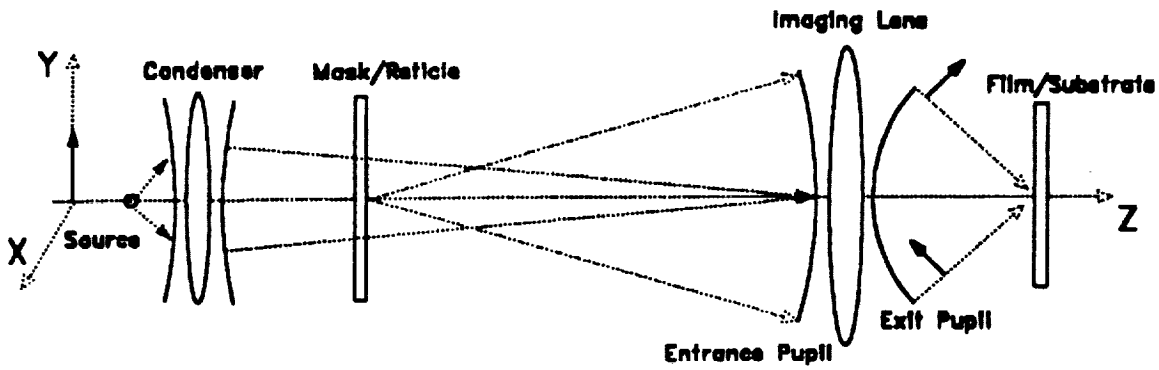

Fig. 2. General Kohler illuminated projection system.

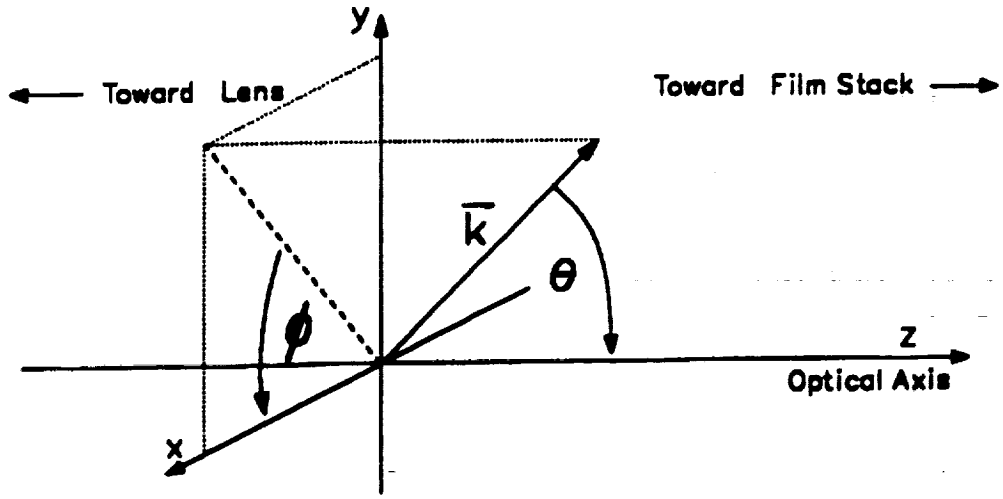

Fig. 3. Coordinate system used to define the projection vector, $\vec{k}$.

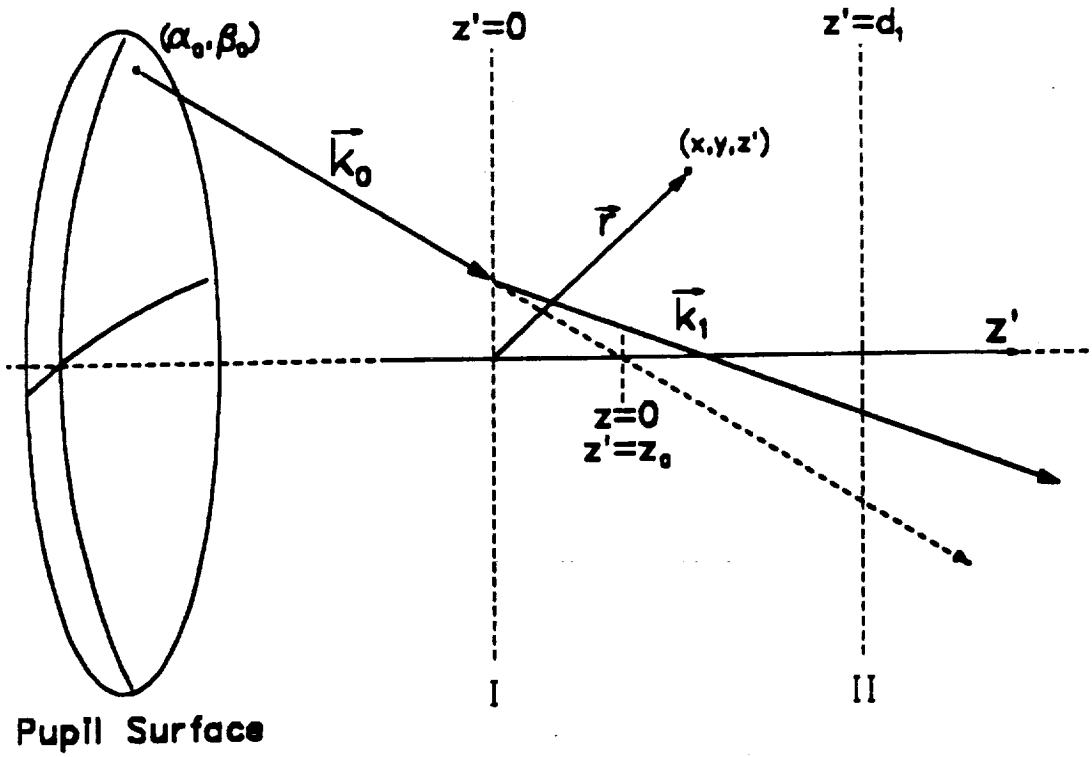

Fig. 4. Schematic of a plane wave propagation vector and position vectors in reference to the pupil and the first thin film.

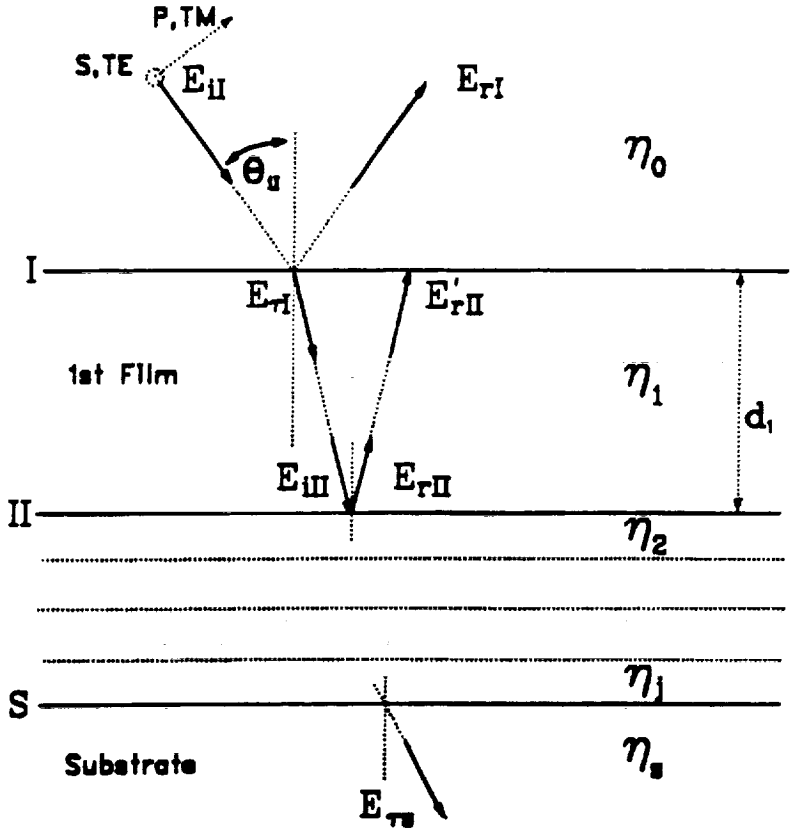

Fig. 5. Diagram of thin film stack with incident plane wave directions and electric field amplitudes.

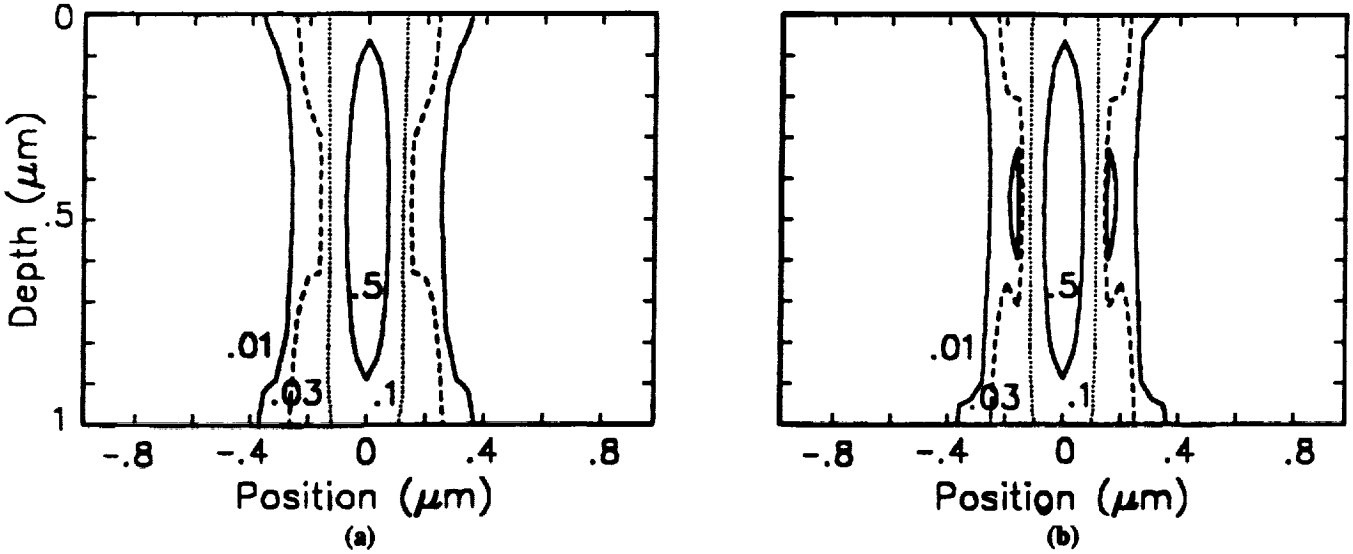

Fig. 6. Iso-irradiance contours of a point image in a $1\mu m$ photoresist film of $\eta_1 = 1.8$ on a matched substrate for a 0.95 NA system, $\lambda = 248nm$, and an initial polarization along the y axis. Meridional slices along (a) y axis, (b) x axis.

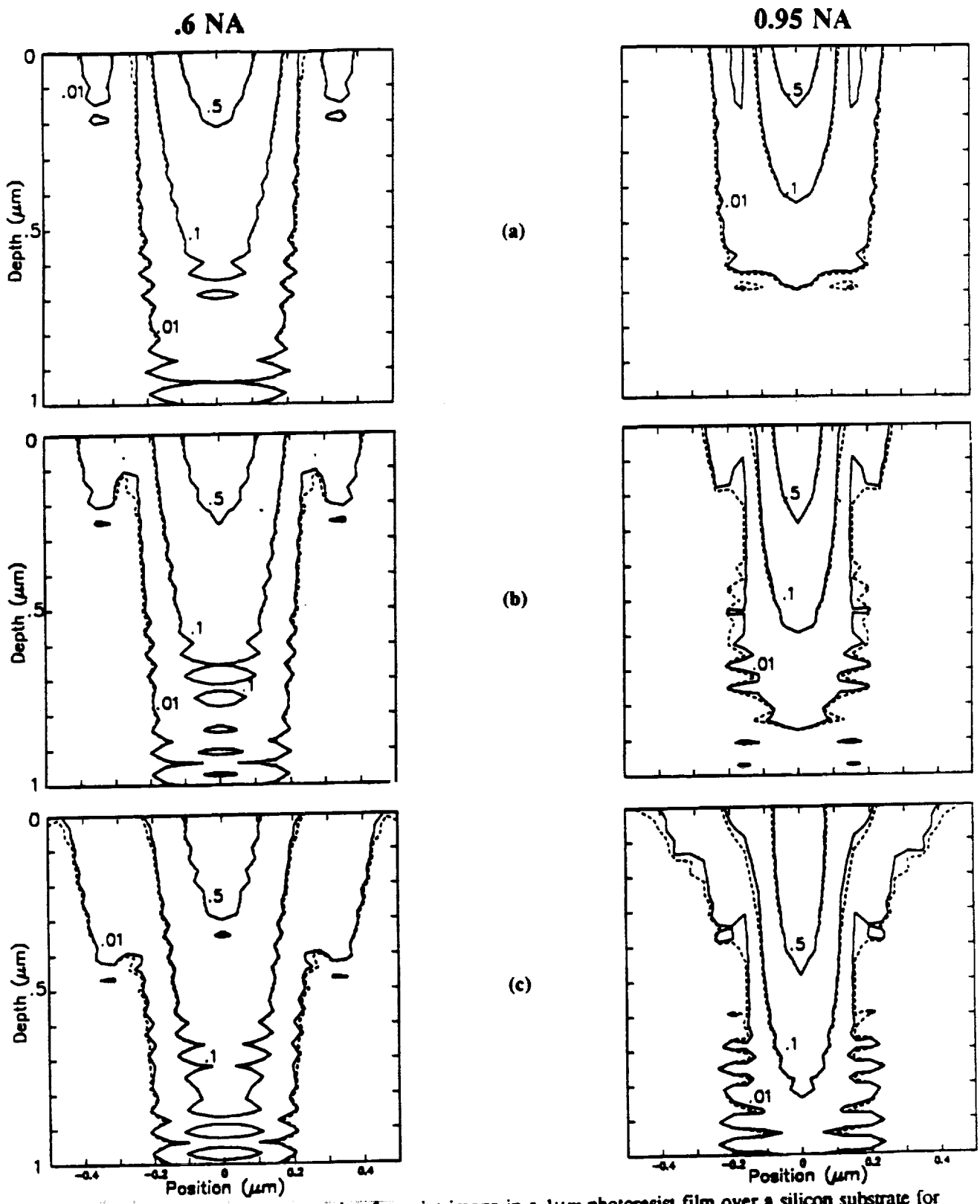

Fig. 7. Iso-irradiance contours in of a point image in a 1μm photoresist film over a silicon substrate for 0.6 and 0.95 NA. The source is initially y polarized and $\lambda = 248nm$ The solid line is a meridional slice along the y axis and the dotted line is a slice along the x axis. Marginal ray focus at (a) 0μm depth, (b) 0.5 μm depth, (c) 1.0μm depth.

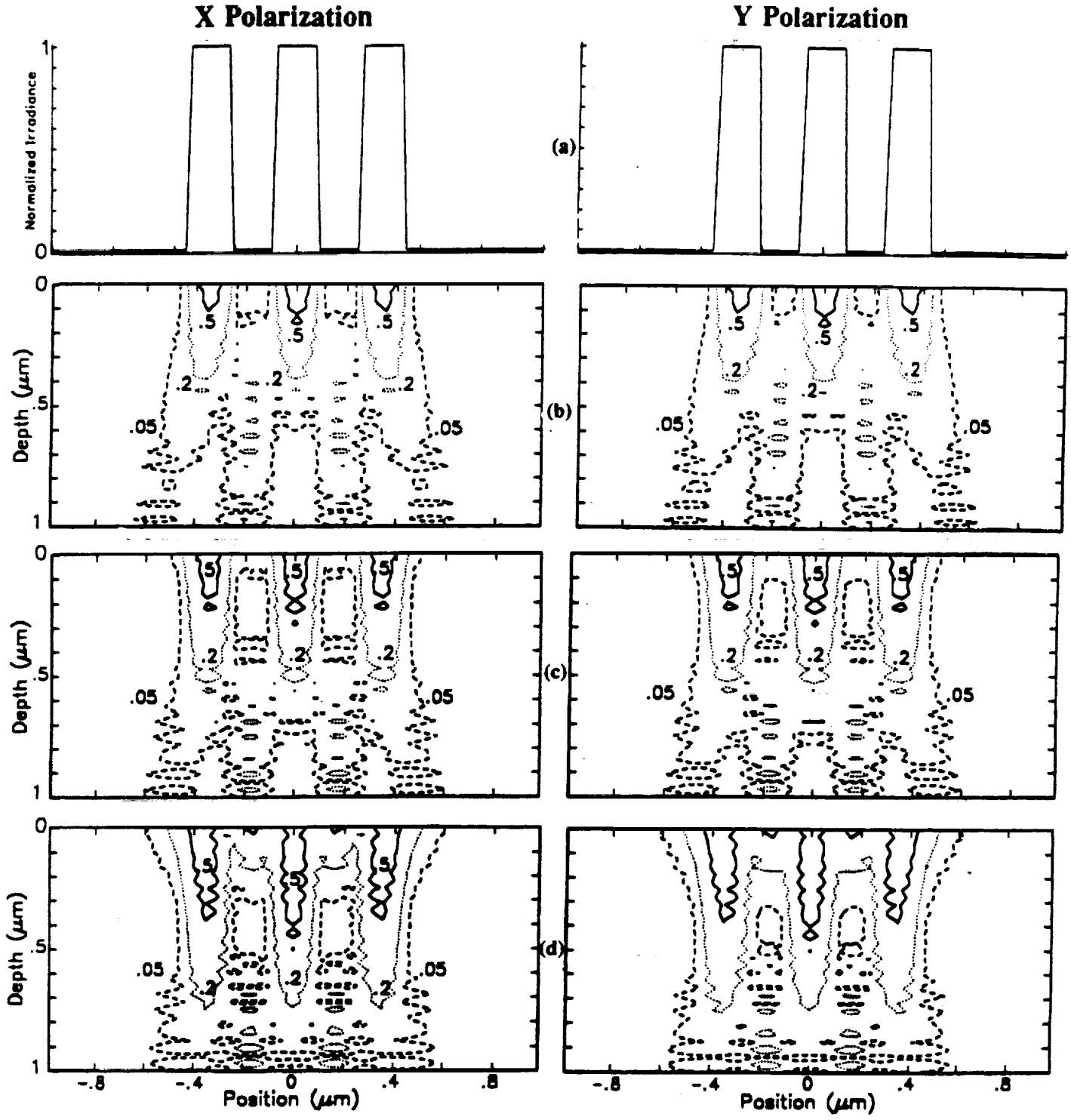

Fig. 8. (a) Transmission function of tri-bar object with lines and spaces parallel to x axis. y meridional slice images of 0.95 NA system with initial x and y polarizations for marginal ray focus at (b) 0μm depth, (c) 0.5μm depth, and (d) 1.0μm depth.

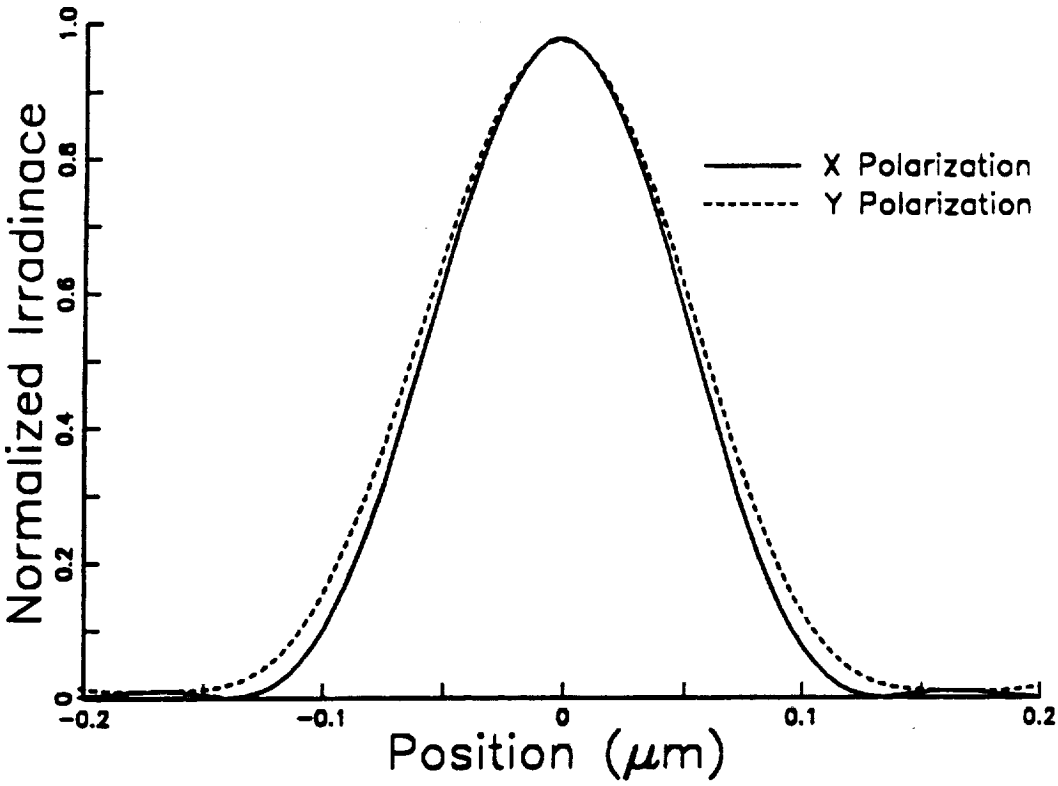

Fig. 9. Plots of irradiance for x and y polarizations at the top surface of the film for a zero offset using the parameters in Figure 8b.

Table I

$\vec{P}(\alpha, \beta)$ Components	Initial Polarization State X	Y
P_{xS}	$\frac{\beta^2}{1-\gamma^2}$	$\frac{-\alpha\beta}{1-\gamma^2}$
P_{xP}	$\frac{\gamma\alpha^2}{1-\gamma^2}$	$\frac{\alpha\beta\gamma}{1-\gamma^2}$
P_x	$1-\frac{\alpha^2}{1+\gamma}$	$\frac{-\alpha\beta}{1+\gamma}$
P_{yS}	$\frac{-\alpha\beta}{1-\gamma^2}$	$\frac{\alpha^2}{1-\gamma^2}$
P_{yP}	$\frac{\alpha\beta\gamma}{1-\gamma^2}$	$\frac{\gamma\beta^2}{1-\gamma^2}$
P_y	$\frac{-\alpha\beta}{1+\gamma}$	$1-\frac{\beta^2}{1+\gamma}$
P_{zP}	$-\alpha$	$-\beta$
P_z	$-\alpha$	$-\beta$

APPENDIX I